Global and Planetary Change 128 (2015) 1–13

Contents lists available at ScienceDirect

Global and Planetary Change

journal homepage: www.elsevier.com/locate/gloplacha

Region-wide glacier mass budgets and area changes for the Central Tien Shan between ~1975 and 1999 using Hexagon KH-9 imagery

Tino Pieczonka [a,*], Tobias Bolch [a,b]

[a] Institute for Cartography, Technische Universität Dresden, 01069 Dresden, Germany
[b] Department of Geography, University of Zurich, 8057 Zürich, Switzerland

ARTICLE INFO

Article history:
Received 3 August 2014
Received in revised form 24 November 2014
Accepted 26 November 2014
Available online 3 December 2014

Keywords:
change assessment
geodetic glacier mass budget
glacier area change
Central Tien Shan
KH-9 Hexagon
Sary-Djaz/Aksu

ABSTRACT

The meltwater released by the glaciers in the Central Tien Shan feeds in particular the Tarim River which is the main artery for the oases at the northern margin of the Taklamakan desert. The correct assessment of the contribution of the glaciers' meltwater to the total runoff is hampered by the lack of long-term measurements of glacier mass budgets. Digital terrain models (DTMs) for the different regions in the Central Tien Shan were generated based on ~1975 KH-9 Hexagon imagery and compared to the SRTM3 DTM acquired in February 2000. Moreover, glacier area changes for the period ~1975–2008 have been measured by means of multi-temporal optical satellite imagery.

The geodetic mass budget estimates for a glacierized area of 5000 km^2 revealed increasing mass loss east to west and from the inner to the outer ranges. Highest mass loss accompanied by the most pronounced glacier retreat was found for the Ak-Shirak massif with a region-wide mass balance of -0.51 ± 0.36 m w.e. a^{-1} and a rate of area change of $-0.27 \pm 0.15\%$ a^{-1}, whilst moderate mass loss was observed for the Inylchek (0.20 ± 0.44 m w.e. a^{-1}) and Tomur area (0.33 ± 0.30 m w.e. a^{-1}) despite partly debris cover. These latter regions also revealed the lowest glacier shrinkage within the entire Central Tien Shan. The total glacier mass loss of 0.35 ± 0.34 m w.e. a^{-1} is, however, within the global average whilst the glacier area shrinkage is comparatively low. On average, the investigated glacierized area of ~6600 km^2 shrank by $0.11 \pm 0.15\%$ a^{-1} only. We could also identify several surge-type glaciers. The results are consistent with in-situ mass balance measurements for Karabatkak Glacier and previously published results of the Ak-Shirak range proving the suitability of declassified imagery for glacier change investigations. The contribution to the runoff of Aksu River, the largest tributary of the Tarim River, due to glacier imbalance has been determined at ~20% for the 1975–2000 period.

1. Introduction

The Tien Shan accommodates several thousand glaciers in the Uzbek, Kyrgyz, Kazak and Chinese part covering an area of about 16,400 km^2 (Kotlyakov et al., 2010), which are an important source of freshwater for the surrounding arid regions (Sorg et al., 2012; Unger-Shayesteh et al., 2013). Central Tien Shan glaciers receive most of their accumulation during summer as precipitation is concentrated between May and September (Kutuzov and Shahgedanova, 2009).

Observations at the Tien Shan meteorological station at 3614 m a.s.l. revealed a continuous increase in mean annual summer air temperature between 0.01 °C a^{-1} (Aizen et al., 1997a [1940–1991 period]) and 0.03 °C a^{-1} (Kutuzov and Shahgedanova, 2009 [1956–2007 period]) and a decrease in annual precipitation between the 1960s and 1990s (Kutuzov and Shahgedanova, 2009; Kriegel et al., 2013).

Therefore, glacier downwasting was the dominating process in the last decades, except for a short period around 1970, when mass gains could be observed for few glaciers based on aerial photography and glaciological observations (Bolch, accepted for publication; Dyurgerov, 2010; Aizen et al., 2007).

Several studies revealed a decrease in glacier area in the Inner and Central Tien Shan between 13% in the Terskey Ala-Too (Khromova et al., 2014; Kutuzov, 2012; Kutuzov and Shahgedanova, 2009 [1965–2003 period]), 23% in the Naryn Catchment (Kriegel et al., 2013 [between 1970s and mid-2000s]), and only 1.3% in the Chinese part (Shangguan et al., 2009 [between mid-1960s and 2000]) showing increasing area losses east to west and from the inner to the outer parts. However, glacier area changes show a delayed response and only the glacier mass budget shows an almost direct signal to climate (Oerelemans, 2001).

Comprehensive analyses of glacier elevation changes are of uttermost importance in order to gain a better understanding on the recent changes in the Central and South Asian ice cover with regard to the ongoing climate change (Marzeion et al., 2014) and for the correct

* Corresponding author at: Institute for Cartography, Helmholtzstraße 10, 01069 Dresden, Germany. Tel.: +49 35146333281; fax: +49 35146337028.
E-mail address: t.pieczonka@tu-dresden.de (T. Pieczonka).

http://dx.doi.org/10.1016/j.gloplacha.2014.11.014
0921-8181/

assessment of the contribution of the glaciers' meltwater to the total runoff (Sorg et al., 2012) and sea-level rise (Gardner et al., 2013). Region-wide geodetic mass balance studies based on national digital terrain models (DTMs) and remote sensing data have been accomplished e.g. for British Columbia (Schiefer et al., 2007), for the Swiss Alps (Paul and Haeberli, 2008), for Alaska (Berthier et al., 2010), and for the Pamir–Karakoram–Himalaya (Gardelle et al., 2013). In contrast, there are few mass balance studies focusing on single glaciers or small catchments only for the Central (Shangguan et al., 2014; Pieczonka et al., 2013; Wang et al., 2013) and Inner Tien Shan (Kutuzov, 2012; Aizen et al., 2007; Surazakov and Aizen, 2006) which may not adequately represent the wide range of glacier behavior in the region.

Several existing in-situ mass balance measurements in the Tien Shan were interrupted in the 1990s after the collapse of the Soviet Union and new investigations have just started or are planned. Longest in-situ mass balance time series exists for Urumqi Glacier No. 1 in the Eastern Tien Shan and Tuyuksu Glacier located in the Northern Tien Shan (WGMS, 2013). Region-wide mass balance estimates for the Tien Shan have recently been determined by means of gravimetric (Jacob et al., 2012) and laser altimetry (Gardner et al., 2013) measurements. These measurements are, however, averaged over the entire Tien Shan and limited to the 2003–2009/2010 period. The declassification of U.S. reconnaissance imagery from the 1960s and 1970s offers huge potentials to compare the state of the glaciers over more than four decades (Pieczonka et al., 2013; Bolch et al., 2011; Lamsal et al., 2011; Surazakov and Aizen, 2010).

The main objective of this study is to assess the region-wide glacier mass budgets for the Central Tien Shan, the most heavily glacierized part of the entire mountain range comprising ~6600 km^2 of ice cover (Arendt et al., 2012). One focus is on the Aksu Catchment whose glacier melt water is of high importance for the Tarim River (Xinjiang/China)—one of the longest cohered intracontinental river systems in the world and of high importance for the economic development of the oases at the northern margin of the Taklamakan desert—which is significantly nourished by glacier melt (Sorg et al., 2012; Kaser et al., 2010).

Roughly 70% of the total runoff is contributed by its largest tributary the Aksu River (Sary-Djaz in Kyrgyzstan) (Wang et al., 2003). Thus, the water supply considerably depends on the glacial meltwater and is therefore influenced by glacier changes.

In addition, we aim to extend the work by Osmonov et al. (2013), who investigated glacier area changes for the 1990–2010 period for the Sary-Djaz Catchment only, both in space and time and to provide information about area changes and relate them to mass changes.

The study region is covering the Aksu Catchment, and parts of the Naryn, Issyk-Kul, Ili, and Muzat Catchment with an area of about 65,000 km^2 where ~10% are ice-covered (Fig. 2). It comprises the Ak-Shirak massif, the Jengish Chokusu (Tomur Feng/Pik Pobeda)—Khan Tengri massif, the Xuelian Feng (Snow Lotus Peak) massif, and parts of the Terskey Ala-Too and KokShal-Too with large compound-valley glaciers, e.g. Tomur or Inylchek glacier, and dendritic glaciers, e.g. Kaindy or Koxkar Glacier whose termini are often debris-mantled (Fig. 3). About ~5% of all glaciers in the area under investigation reveal a layer of debris. Debris-covered glacier tongues are characterized by exposed ice cliffs and supraglacial ponds which significantly influence the overall glacier mass budget (Juen et al., 2014; Sakai et al., 2000). Glaciers in the study region are typically polythermal or cold (Osmonov et al., 2013; Shi and Liu, 2000).

2. Data

Remote sensing data were selected in terms of complete ground coverage. Therefore, we selected KH-9 Hexagon imagery and the almost globally available SRTM3 dataset for elevation change assessments. In addition, we used Landsat MSS, TM and ETM+ as well as SPOT-5 data for generating a glacier inventory and performing change assessments (Fig. 1, Table 1).

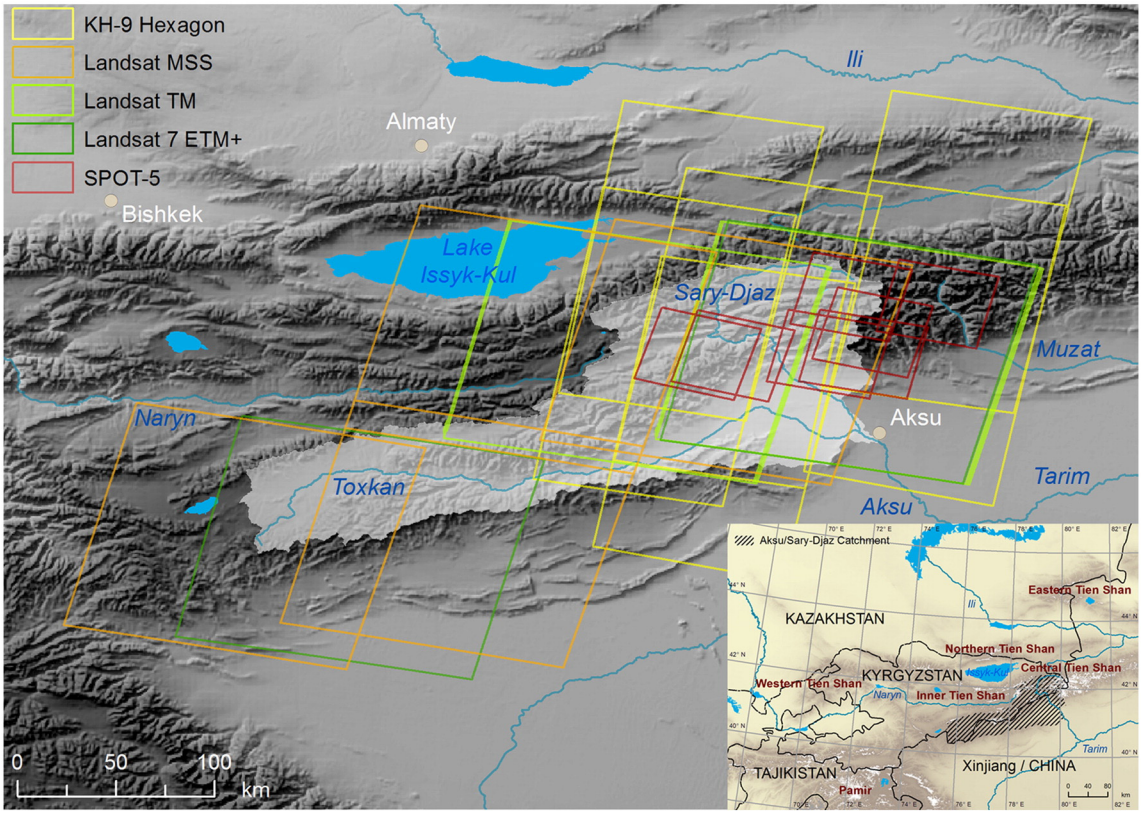

Fig. 1. Data coverage of the utilized datasets for glacier delineation and DTM processing.

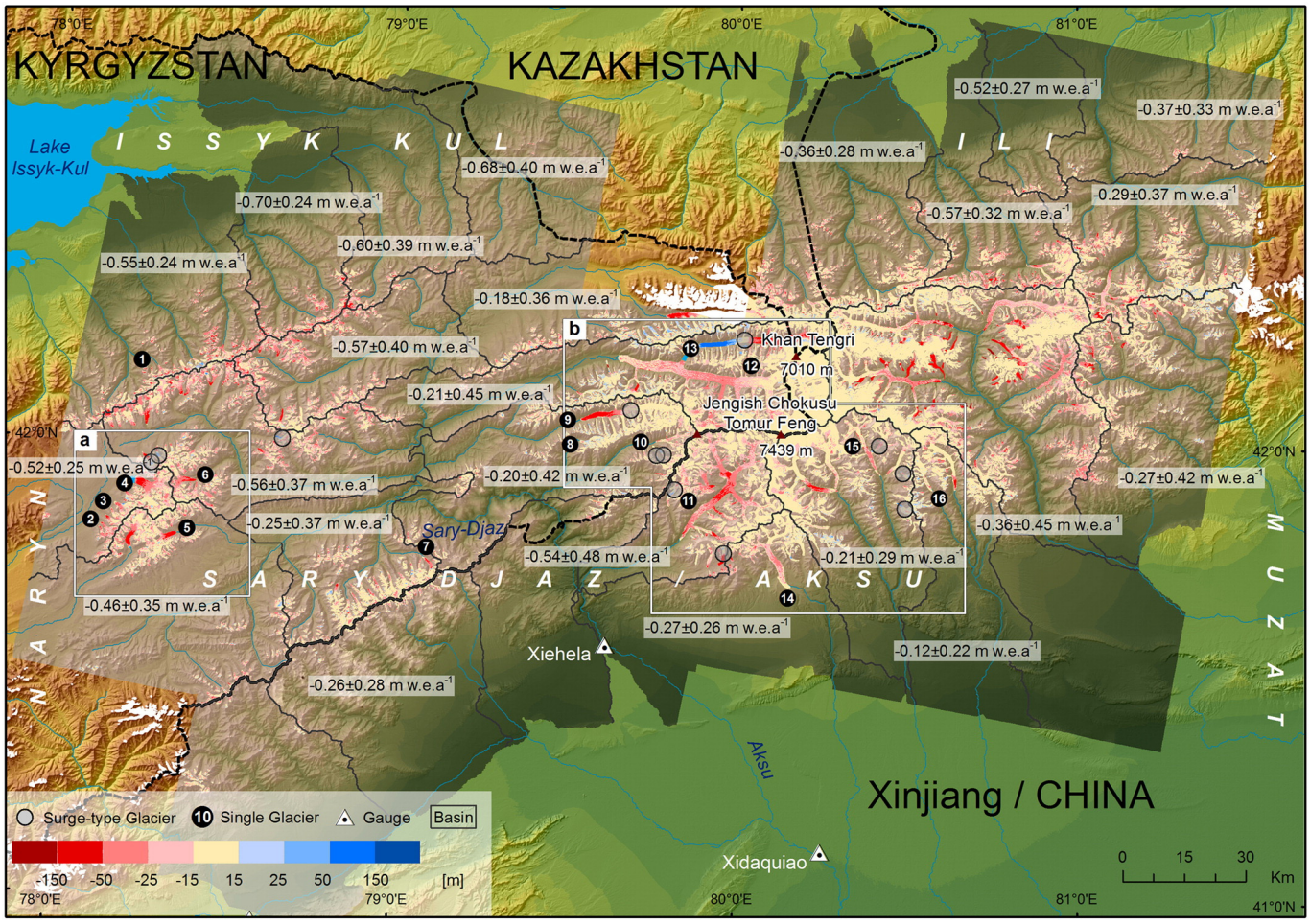

Fig. 2. Study region showing the coverage of the KH-9 DTMs and the calculated glacier elevation differences. Detailed maps (cf. Fig. 7) have been generated for the Ak-Shirak and Tomur–Inylchek region. Glacier mass budgets for single basins (depicted as gray polylines) reveal spatial heterogeneity.

2.1. KH-9 Hexagon—Mapping Camera (MC)

KH-9 Hexagon, whose images were declassified in 2002, was part of the US keyhole reconnaissance satellite program. However, detailed lens distortion information were not declassified with the film. The Mapping Camera (MC) System operated between April 1973 (Mission 1205) and June 1980 (Mission 1216). During this time about ~209,000 km^2 were recorded in trilap mode, ~60,000 km^2 in bilap mode and ~63,000 km^2 in mono mode. The utilized 12-inch terrain lens system, with a maximum distortion of 26 μm and a field of view of 80°, enabled a 129 × 259 km^2 ground coverage on a scale of 1:600,000 at an altitude of ~170 km (perigee) (Burnett, 2012). Due to the frame camera design Hexagon images are characterized by four fiducial marks and 1081 reseau crosses (Surazakov and Aizen, 2010), which can be used to restore the image geometry at the time of image acquisition. For the KH-9 missions the same film as for the KH-4

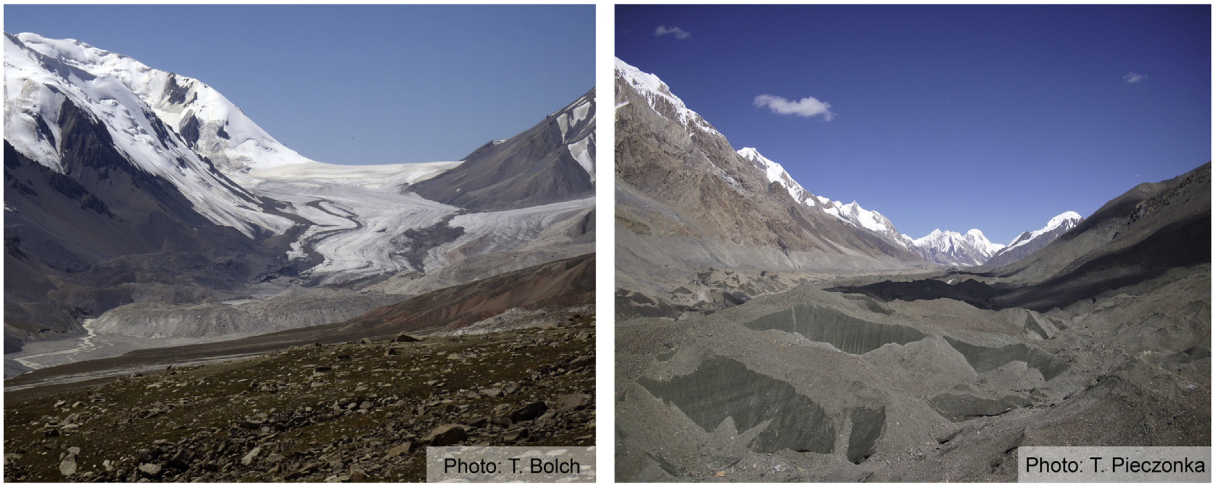

Fig. 3. Photographs of Kaindy Glacier in the Ak-Shirak massif [left] and Kaindy Glacier in the Tomur–Inylchek region [right] taken in August and September 2012.

Table 1
Input and reference datasets.

Sensor	Date	ID/path-row	Spatial res.	Usage
KH-9 Hexagon	31/07/1973		7.6 m	Glacier mass budget + mapping (P)
KH-9 Hexagon	16/11/1974		7.6 m	Glacier mass budget + mapping (P)
KH-9 Hexagon	12/01/1976		7.6 m	Glacier mass budget + mapping (P)
Landsat MSS	12/08/1975	159/031	60 m	Glacier mapping (S)
Landsat MSS	13/08/1975	160/031	60 m	Glacier mapping (S)
Landsat MSS	03/08/1977	161/032	60 m	Glacier mapping (S)
Landsat MSS	08/08/1978	160/032	60 m	Glacier mapping (S)
Landsat TM	08/08/2007	147/031	30 m	Glacier mapping (P)
Landsat TM	16/09/2007	148/031	30 m	Glacier mapping (P)
Landsat TM	16/08/2010	147/031	30 m	Glacier mapping (S)
Landsat ETM+	18/02/2000	147/031	15 m	Snow mapping
Landsat ETM+	22/08/2010	149/032	15 m	Glacier mapping (S)
SPOT-5	24/08/2007	206/265	2.5 m	Glacier mapping (S)
SPOT-5	18/09/2007	203/266	2.5 m	Glacier mapping (S)
SPOT-5	19/09/2007	204/265	2.5 m	Glacier mapping (S)
SPOT-5	01/02/2008	204/265	2.5 m	Glacier mapping (S)
SPOT-5	30/07/2009	202/265	2.5 m	Glacier mapping (S)
SPOT-5	02/11/2009	205/265	2.5 m	Glacier mapping (S)
SPOT-5	04/09/2010	205/265	2.5 m	Glacier mapping (S)
SRTM (STS-99)	11/02/2000		~90 m	Glacier mass budget

P … Primary scene, S … Secondary scene.

mission, which was the first mission providing stereo coverage, with a film resolution of about 85 lp/mm (line pairs per millimeter) was used. KH-9 imagery is preferred, as one KH-9 scene covers an area of 250 × 125 km^2, whereas the footprint size of one KH-4 filmstrip is only 15 × 210 km^2 accompanied by complex panoramic distortions making the stereo-processing more difficult (Pieczonka et al., 2011).

A scan resolution of about 4000 dpi is needed to get the image content without any loss of information. Due to scratches on the images as a consequence of the long time of storage and for performance reasons we decided to use the data with a scan resolution of 14 micrometer (1800 dpi) scanned by USGS Earth Resources Observation and Science (EROS) Center. Three KH-9 MC stereopairs with 70% overlap acquired in mission 1206 (1973), 1209 (1974), and 1211 (1975) were processed for DTM generation. The Hexagon data cover most parts of the study region except the westernmost parts (Fig. 2).

2.2. Landsat/SPOT data

Data from the Landsat Mission provide a unique archive of satellite imagery since the 1970s. It all started with the 4-channel Multi-Spectral Scanner (MSS) operating in the visible and near-infrared-(VNIR) spectrum having a spatial resolution of 79 m. Since the fourth Landsat mission launched in 1984 the TM sensor, also equipped with two short-wave infrared (SWIR) sensors, has acquired images with an improved resolution of 30 m which allowed for the first time automated mapping of snow and ice. The SPOT-1 satellite, operated by the Centre national d'études spatiales (CNES), was launched in 1986 and had beside 4 VNIR (visible and near-infrared) bands a panchromatic band with a geometric resolution of 10 m. Since 2002 SPOT-5 has been acquiring imagery with a spatial resolution of 2.5 m. For this study, the best available Landsat TM scenes from the period 2007–2010 were downloaded from the USGS GLOVIS website (glovis.usgs.gov). Snow conditions were suitable for most of the scenes except for the central part of the study area where the highest peaks are located. Therefore, we used two scenes with different snow conditions in different parts of the scenes complemented by pansharpened SPOT-5 data recorded between 2007 and 2010 with a spatial resolution of 2.5 m covering an area of 60 × 60 km^2. Landsat MSS data from the years 1975–1978 were used to obtain information about the glacier extents from the 1970s were Hexagon data was not available (Table 1). Landsat data were available in the orthorectified level 1 T whilst SPOT-5 data have been orthorectified using GCPs obtained from Landsat ETM+ scenes and the SRTM3 DTM.

2.3. SRTM3 digital terrain model

The SRTM3 dataset, which has an absolute horizontal accuracy of 20 m and a vertical accuracy of up to 10 m (Rodriguez et al., 2006) with increasing inaccuracies towards steeper terrain (Racoviteanu et al., 2007; Jacobsen, 2005), was chosen as vertical reference for GCP collection. Because the original SRTM3 datasets suffer from radar related data gaps in high mountain regions we used the gap-filled SRTM3 DTM from the Consultative Group on International Agricultural Research (CGIAR) Version 4.1 (Jarvis et al., 2008)—resampled to 25 m in a bicubic manner in order to preserve the elevation structure of the original DTM (Xiuping and Richards, 1999)—as master for the co-registration of the Hexagon KH-9 DTMs. The non-filled SRTM3 DTM was used for the calculation of the glacier elevation differences.

3. Methodology

3.1. Glacier mapping

Parts of our glacier inventory are based on glacier outlines of the period ~2008 generated by Osmonov et al. (2013) for the Sary-Djaz basin and Pieczonka et al. (2013) for the Tomur region which cover ~40% of the studied glacier area but less than one third of the glacier number. Glaciers in the regions to the east, west and south have been mapped automatically based on the well-established Red/SWIR band ratio (Paul et al., 2014; Bolch et al., 2010) using Landsat TM images. The outlines were visually checked and, if available, manually adjusted in terms of seasonal snowpatches and missing debris-covered glacier parts using the high resolution SPOT-5 scenes as supplementary information. We also identified few debris-covered glacier parts missing and some wrongly mapped seasonal snow in the Sary-Djaz inventory (Osmonov et al., 2013). However, overall this inventory is of good quality and the omission and commission areas were only about 0.5%. The contiguous ice masses were separated into single glaciers based on hydrological basins following Bolch et al. (2010). The 2007–2010 outlines served as a basis for the manual adjustment for the 1970s using the KH-9 Hexagon and Landsat MSS scenes.

The precision of the automated delineation is commonly within half a pixel with regard to the glacier perimeter (Paul et al., 2013; Bolch et al., 2010). Consequently, the mapping uncertainty was calculated using a buffer of 10 m taking into consideration that higher resolution datasets were available for manual improvements. For the 1970s outlines we

assumed a mapping inaccuracy of 1 pixel (~8 m in terms of the spatial resolution of KH-9 imagery) and 30 m (i.e. half a MSS pixel) for the parts where only MSS data was available. This led to an uncertainty of 3.0% for the ~2008 data and 3.8% for the ~1975 data which matches well the uncertainty revealed in other studies (Paul et al., 2013; Bolch et al., 2010; Paul et al., 2002). The overall uncertainty for the area change was 4.8% considering the law of error propagation.

Because an insufficient amount of Landsat scenes of good quality was available for the period around 2000 the inventory was generated with the glacier area as constituted around the year 2008.

3.2. KH-9 Hexagon processing

All KH-9 DTMs were generated with LPS (Leica Photogrammetry Suite) 2013 using the frame camera model with a fixed focal length of 30.5 cm. The pre-processing of the KH-9 images, comprising the removal of internal film distortions based on reseau crosses, has been done following Pieczonka et al. (2013). GCPs have been collected from Landsat 7 ETM+ imagery (15-meter panchromatic band) with SRTM3 as vertical reference. The coordinates of the fiducials were measured manually starting from the image center. All stereopairs have been processed with a RMS of triangulation of <~1 Pixel (Table 2). The spatial resolution of the final DTMs was 25 m.

Both, the KH-9 mapping camera (MC) and the Large Format Camera (LFC) have a similar camera design with comparable maximum lens distortions of about 26 μm (Burnett, 2012; Surazakov and Aizen, 2010). Therefore, we transferred the radial lens distortion of the LFC camera (Mollberg and Schardt, 1988) to the KH-9 MC camera.

To account for any tilt between two DTMs the global trend of elevation differences between $-150\ m \le \Delta h \le 150\ m$ over gently inclined ($\le 15°$) non-glaciated terrain was calculated and added to the KH-9 DTM. In order to avoid including unmapped glacier pixel in our non-glaciated terrain we chose a glacier mapping error of 3 pixels.

Then we subdivided the entire study region into single basins. This gave us the possibility to better consider local horizontal and vertical deviations for an optimal co-registration. In total, we deduced 24 basins covering an area between 650 and 2700 km^2. Subsequently, all subset DTMs were co-registered following the approach described by Nuth and Kääb (2011) and Pieczonka et al. (2013). The final displacement vectors between KH-9 Hexagon and SRTM3 were less than or equal one pixel (25 m) on average.

3.3. Data gaps and outlier handling

Data gaps mainly occur in areas with less image contrast when working with optical imagery. In high mountain areas this is mainly related to the snow-covered accumulation regions and areas with cast shadows. Together with radar induced data gaps the proportion of missing information on glaciers is comparatively high with ~30% over the entire study region. The missing values predominantly occur in the eastern part, where the original SRTM3 shows large data gaps.

Outlier filtering was necessary for both the non-glaciated terrain which is an indicator for the quality of the co-registration as these areas are supposed to be stable over time, and for the glaciers where the non-filtered difference image revealed peaks of surface lowering in the accumulation regions due to mismatched pixels.

For the ice-free terrain, outliers are defined by the 1.5 fold interquartile range (IQR). We calculated the NMAD (Normalized Median Absolute Deviation) for stable terrain for all single basins as a robust estimator for the standard deviation (Pieczonka et al., 2013). The overall accuracy for the entire study region has then been determined as the NMAD of all weighted NMAD values for all basins.

Outliers on glaciated terrain have been filtered under the assumption that thickness change distributions for glaciers with negative budgets typically have maximum lowering on the glacier front and lowest downwasting at higher altitudes following a non-linear trend (Schwitter and Raymond, 1993). However, this typical pattern is altered by debris cover and does not consider special forms like surge-type glaciers with high frequencies of extremly positive Δh values on comparatively low altitudes. Thus, heterogeneous glacier thickness changes with volume gains and volume losses in ablation regions made it difficult to apply a general threshold to the entire glaciated terrain in order to remove outliers. Therefore, we decided to filter in dependence on the overall standard deviation of the glacier elevation differences weighted by an elevation dependent coefficient. With respect to the non-linear behavior of glacier thickness change the weighting coefficient has been determined using a sigmoid function (Eq. (E2)) which is supposed to be a good reflection of the elevation dependency. For this purpose, we first normalized the elevation of all glacier pixels by the maximum elevation range (Eq. (E1)). In the second step the weighting coefficient (r_{STD}) has been determined using Eq. (E2) with w as the normalized glacier elevation. We found that the tenfold standard deviation was suitable in order to preserve glacier surges. E2 was adapted accordingly resulting in a maximum value of 10 and a minimum of 0.02 for the highest elevations where only small glacier thickness changes are expected. Thus, the weighting coefficient r_{STD} which has finally been multiplied with the overall standard deviation of the glacier elevation differences afflicted with outliers is small ($r_{STD} \ll 1$) for high altitudes and large in the ablation regions ($r_{STD} \gg 1$) warranting a larger range of Δh values in the less steep ablation regions to preserve surge-type glaciers and a narrow range of Δh values ($-0.5 \le \Delta h \le 0.5$ m) at the glacier head (Fig. 4).

$$w = \frac{(Max_{Elevation} - Min_{Elevation})}{Glacier_{Elevation}} \quad \text{(E1)}$$

$$r_{STD} = 5 - 5\tanh(2\pi - 5w) \quad \text{(E2)}$$

$$\Delta h_{max} = r_{STD} * STD_{Glacier} \quad \text{(E3)}$$

w…normalized glacier pixel elevation
$Max_{Elevation}$…maximum glacier elevation, $Min_{Elevation}$…minimum glacier elevation
r_{STD}…weighting coefficient
Δh_{max}…maximum thickness change, $STD_{Glacier}$…overall standard deviation of glacier Δh

All missing pixel values in the ablation and accumulation regions were filled by means of ordinary kriging. Kriging was accomplished without anisotropy modeling assuming a stationary variance but also a non-stationary mean value within the search radius. However, huge amounts of radar induced data gaps in the SRTM3 DTM east of Khan Tengri impaired the filling and boundary effects are still visible (Fig. 2).

3.4. Radar penetration

Radar penetration for the C-band of SRTM is supposed to be highest in the accumulation regions, where snow and firn is prevailing (Rignot et al., 2001). We determined the penetration depth of the C-band signal by comparing our SRTM3 elevations with available ICESat GLA14 footprints following the approach described by Kääb et al. (2012). Due to the C-band penetration SRTM3 is likely referring to the end of summer 1999 glacier surface. Therefore, in order to allow a direct comparison to SRTM3 elevations we only selected footprints captured between September and October assuming that they are representing the surface at the end of the ablation season of the respective year.

All footprints have than been co-registered to SRTM3 and the SRTM3 elevations were bilinearly resampled. The shift vector in x-direction was

Table 2
Amount of GCPs and residuals of stereo image processing in LPS 2013.

	KH-9 Ak-Shirak	KH-9 Kaindy	KH-9 Koxkar
No. GCPs	40	38	47
RMSE [pixel]	0.5	0.8	1.1

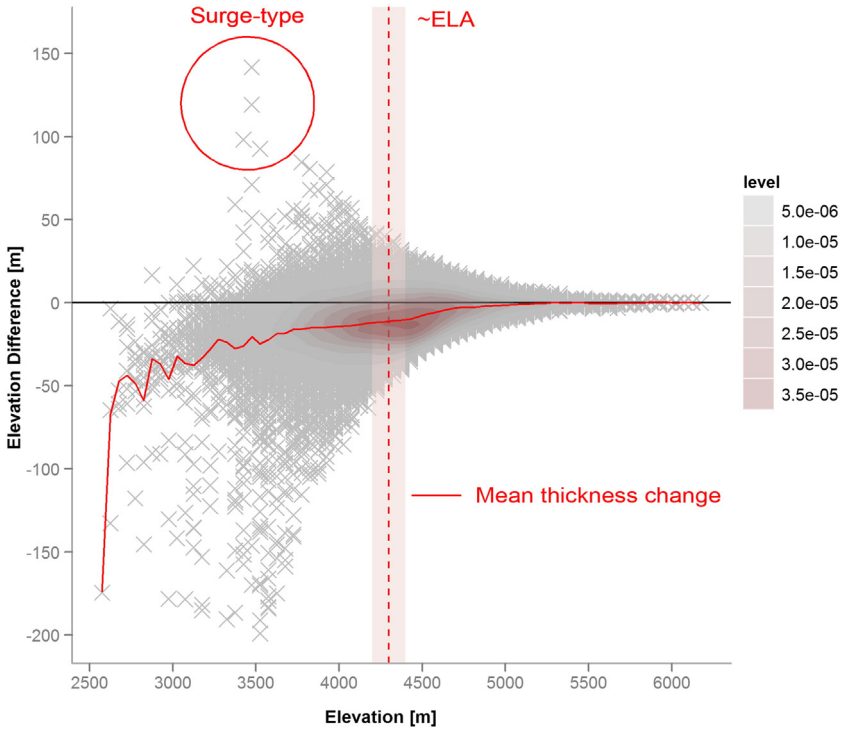

Fig. 4. Distribution and 2D density of mean elevation differences for glaciated terrain after outlier-cleaning within 50 m elevation bands calculated for each individual glacier. The range of the appearing ELA values—derived from snow line values specified in the Katalog Lednikov SSSR [Glacier Inventory of the USSR] (1973)—is illustrated as a buffer of ± 100 m. Positive values of up to + 150 m in lower altitudes are indicators of surge-type glaciers and glacier thickening.

0.6 m and 14.7 m in y-direction. Erroneous ICESat elevations caused e.g. by clouds were eliminated by applying a threshold of ± 150 m to the calculated elevation differences. Since the analysis is hampered by different geometric resolutions of both datasets (90 m vs. 70 m) we also eliminated all values on steep terrain (slope angle > 30°). In a last step we classified the footprints into non-glacier, glacier without debris-cover, debris-cover, and in one class only containing pixel in accumulation regions. As ICESat was launched in 2003 the 1999 penetration depth was extrapolated by a robust linear regression based on the mean elevation differences of the available 2003–2009 tracks and corrected by the non-glacier median offset of 0.43 m. The uncertainty of the penetration depth was evaluated based on the standard error for each class (Kääb et al., 2012).

We determined a mean penetration depth of − 2.2 ± 1.2 m for the debris-free glacier regions, − 6.0 ± 2.2 m for the accumulation regions, + 1.8 ± 3.3 m for the debris-covered glacier parts, and − 0.5 ± 0.2 m for the non-glacier area. The positive value for the debris-covered part is likely due to different geometric resolutions but is in agreement with the values reported by Kääb et al. (2012) for the debris-covered regions in the Karakoram. To correct our elevation differences for radar penetration we finally added a constant penetration depth of − 2.2 m to all pixel values in glacierized regions without debris-cover. The uncertainty of ± 1.2 m is considered within the accuracy assessment. The correction for radar penetration decreases the mass budgets by 0.07 m w.e. on average.

3.5. Accuracy assessment

The overall thickness change uncertainty was calculated by Eq. (E4) considering the radar wave penetration accuracy Δp of ± 1.2 m and the relative vertical accuracy $\Delta\sigma$ (NMAD) of non-glacier terrain after DTM co-registration. Assuming an ice density of (ρ_I) 850 kg/m^3 and adding the ice density uncertainty $\Delta\rho$ of 60 kg/m^3 (Huss, 2013) we finally got the overall mass budget uncertainty u_M (Eq. (E5)) where t is the length of the observation period, Δh is the measured glacier thickness change, and ρ_W the density of water (999.972 kg/m^3).

$$u_{DTM} = \sqrt{(\Delta\sigma)^2 + (\Delta p)^2} \tag{E4}$$

$$u_M = \sqrt{\left(\frac{\Delta h}{t} * \frac{\Delta\rho}{\rho_W}\right)^2 + \left(\frac{u_{DTM}}{t} * \frac{\rho_I}{\rho_W}\right)^2} \tag{E5}$$

The comparison with in-situ mass balance measurements necessitates the correction for seasonality. This is true for the KH-9 Hexagon images which were acquired in July 1973, November 1974 and January 1976 and do not coincide with the end of the ablation season (typically end of September).

Winter precipitation in the Central Tien Shan is low, as about ¾ of the annual precipitation occurs between May and September (Kutuzov and Shahgedanova, 2009). At Ts. Tuyuksu Glacier located at the northern edge of the Tien Shan only 8% of the precipitation occurs in winter (DJF) and the portion of winter accumulation should be similar or even less in the Central Tien Shan (Narama et al., 2010; Cao, 1998). As the precipitation is not homogeneous over the entire Central Tien Shan we assumed 15% of precipitation in the glaciological winter (between first of October and end of February; cf. Tien Shan Station and Karabatkak valley station) resulting in a mean winter accumulation rate of 0.1 m w.e. (0.02 m w.e. per winter month) for all glaciers draining into lake Issyk-Kul. This is in agreement with the mean winter precipitation rate at the Karabatkak valley weather station (1699 m a.s.l.) in the 1970–1979 period of 100 mm. With 0.05 m w.e. (0.01 m w.e. per winter month) the mean winter accumulation at the Tien Shan climate station (3639 m a.s.l. [since 1997 3614 m a.s.l.]) is only half of that of Karabatkak Glacier. Hence, a value of 0.01 m w.e. per winter month has been used to correct the mass balances of all glaciers draining into the Sary-Djaz, Muzat, and Naryn. For the glaciers located within the Ili River Catchment a correction of 0.03 m w.e. per winter

month (taking annual precipitation at Ts. Tuyuksu Glacier of about 990 mm [Narama et al., 2010] into account) was used under consideration of higher precipitation in the outer ranges. For the glaciers in the western part (e.g. Ak-Shirak), where KH-9 Hexagon was recorded in July, the correction was set to 0 assuming that ablation and accumulation are balanced. In sum, all final mass budgets are corrected for radar penetration and seasonality.

The standard error of the seasonality correction has been determined with ±0.004 m w.e. which is negligible in terms of the long period of investigation.

Glacier mass budgets are calculated for a sample of 16 single glaciers (Table 5), for all separated catchments (Fig. 2), and for specific mountain ranges (Table 6). Moreover, the influence of debris cover is analyzed.

4. Results

The study presents for the first time information about glacier area and glacier mass changes for a large continuous area using KH-9 Hexagon imagery from the 1970s. In general, glacier changes in the Central Tien Shan are spatially heterogeneous with predominantly retreating and thinning but also advancing and thickening glaciers.

4.1. Glacier area changes

The entire mapped glacierized area with an extension from the Ak-Shirak range in the west to the Bohogo in the east was covering an area of 6607 ± 251 km^2 in ~1975 and 6362 ± 191 km^2 in ~2008 (Table 3). Hence, the overall glacier area shrank by 245 ± 315 km^2 or 3.7 ± 4.8% (or 0.11 ± 0.14% a^{-1}). The area of glaciers draining into Aksu River decreased from 3539 ± 135 km^2 to 3410 ± 102 km^2 (3.6 ± 4.8% or 0.11 ± 0.14% a^{-1}).

The glacier shrinkage was highest in the west (34 ± 18 km^2 or 8.8 ± 4.8% in the Ak-Shirak range) and lowest in the KokShal-Too range (1.6 ± 4.9 km^2 or 1.5 ± 4.8% or 0.05 ± 0.16% a^{-1}) (Fig. 5). In this highly continental range several debris-covered glaciers with transitions to creeping permafrost features (rock glaciers) exist and no visible area changes could be identified here. Glacier shrinkage is also low in the central ranges with the highest peaks and large debris-covered glaciers like Inylchek, Tomur or Koxkar Glacier.

Taken together, the large debris-covered glaciers in the central ranges (Southern Inylchek, Tomur, and Koxkar glacier) covered an area of 802 ± 30 km^2 in 1975 and shrank by only 1.7 ± 4.8% until ~2008. In the same time, the area of Northern Inylchek Glacier increased by ~6.5 km^2 due to a surge which occurred around 1997 (Mavlyudov, 1999). The largest area increase of more than 10% (1975: 5.96 km^2, 2007: 6.63 km^2) could be observed at Samoilowitsch Glacier (Glacier No. 377) where a surge happened after 2000 (Osmonov et al., 2013).

4.2. Glacier mass changes

Glaciers in the Central Tien Shan show predominant downwasting in the ~1975–1999 period with an average thickness decrease of 10.4 ± 9.8 m resulting in an average mass loss of 0.35 ± 0.34 m w.e. a^{-1} (Table 4).

The highest mass loss could be observed for the western and northern catchments with mass budgets between −0.55 ± 0.24 and −0.70 ± 0.24 m w.e. a^{-1}. Moderate rates are concentrated to the areas south and north of Jengish Chokusu/Tomur Feng (Table 6). A similar pattern can also be seen for the single glaciers (Table 5). Sary-Tor Glacier and Bordu-Juschnaja Glacier in the Ak-Shirak massif experienced the highest mass loss of 0.51 ± 0.25 m w.e. a^{-1} and 0.79 ± 0.25 m w.e. a^{-1}. In contrast, the mass loss of North and South Inylchek glaciers and Koxkar Glacier are roughly half as negative as for the glaciers in the Ak-Shirak. A positive mass budget of 0.22 ± 0.42 m w.e. a^{-1} was observed for Bulantor Glacier, a west-oriented valley glacier south of Kaindy Glacier. Keqikekuzibayi Glacier in the Chinese part of the Central Tien Shan revealed a balanced budget of +0.02 ± 0.22 m w.e. a^{-1}.

Surging patterns with a characteristic increase in surface elevation at the end of the glacier tongue and a surface lowering in the upper part could be observed for a couple of glaciers in the Ak-Shirak and Tomur area (Figs. 2, 7). The most pronounced surge was observed for North Inylchek Glacier with a maximum surface increase of ~150 m in the 1974–1999 period (Shangguan et al., 2014) (Fig. 7b). The significant thickening at the end of glacier tongue is due to a surge that happened around 1997 (Mavlyudov, 1999). Some glaciers show a characteristic bulge in the course of their glacier tongue indicating a surge in progress. The strongest glacier lowering as a follow-up of a surge that happened between 1943 and 1960 (Kotlyakov et al., 2010) could be observed for Kaindy Glacier with a maximum downwasting of ~100 m.

To get a broader view over the region we subdivided the study site into certain mountain ranges and larger catchments (Table 6). Here, the mass budgets are strongly influenced by the largest glaciers in the respective division. In the area north of Jengish Chokusu 76% of the entire glacierized area is covered by only 2% of the glaciers with the result that the mean mass budget is similar to that of North and South Inylchek Glacier. In general, the mass budgets of Tomur Area and Aksu Catchment are within the average, whilst the Ak-Shirak shows more negative and the Inylchek Area less negative mass budgets (Table 6, Fig. 6).

Significant downwasting rates could also be found for large debris-covered glaciers, e.g. Tomur Glacier, Kaindy Glacier, and Inylchek Glacier (Table 5). The highest mean downwasting rates for debris-covered glacier parts of more than 1.0 m a^{-1} were measured for Tomur and Kaindy Glacier. An exception is North Inylchek Glacier whose debris-covered part shows a thickening of 0.36 ± 0.53 m a^{-1} which can be traced back to a re-distribution of mass as a consequence of the mentioned surge.

Artifacts induced by data gap interpolation are visible in the basin east of Mount Khan Tengri where the proposed outlier filtering does not work sufficiently. This is because this region was also characterized by the highest amount of missing pixel values in the original SRTM3 DTM. Due to boundary effects and successive interpolation errors, mass losses in the mid-eastern part are suspected to be slightly overestimated.

5. Discussion

Sufficient image contrast is most import when calculating geodetic mass budgets using optical stereo imagery. However, accumulation

Table 3
Glacier area changes between ~1975 and ~2010.

Region	Area ~1975 (km^2)	Area ~2008 (km^2)	Change abs. (km^2)	Change rel. (%)	Change a^{-1} (%)
Ak-Shirak	381 ± 15	348 ± 10	−34 ± 18	−8.8 ± 4.8	−0.27 ± 0.15
KokShal-Too	587 ± 22	577 ± 17	−10 ± 28	−1.6 ± 4.9	−0.05 ± 0.16
Inylchek region	1074 ± 41	1042 ± 31	−32 ± 51	−3.0 ± 4.8	−0.09 ± 0.15
Tomur region	964 ± 37	940 ± 28	−24 ± 46	−2.5 ± 4.8	−0.08 ± 0.15
Aksu Catchm.	3539 ± 135	3410 ± 118	−129 ± 169	−3.6 ± 4.8	−0.11 ± 0.15
All	6607 ± 251	6362 ± 191	−245 ± 315	−3.7 ± 4.8	−0.11 ± 0.15

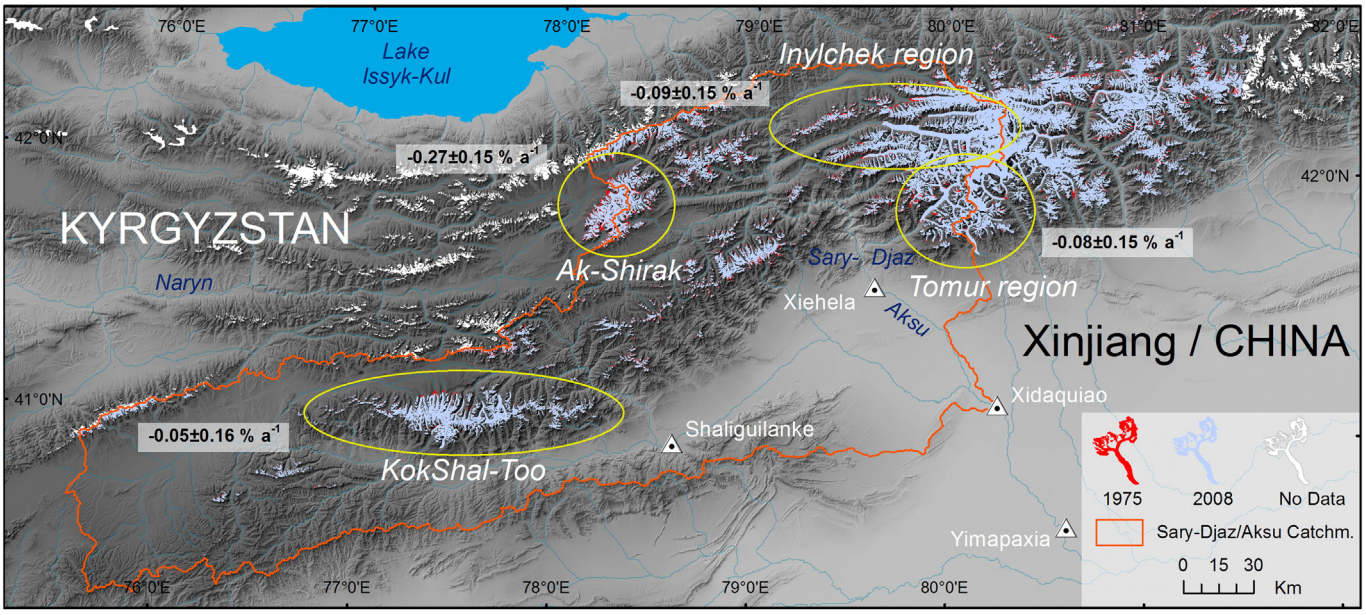

Fig. 5. Glacier area changes in the Central Tien Shan since ~1975 with the most significant glacier area shrinkage in the Ak-Shirak massif.

regions, in particular, suffer from less contrast and large regions without any information content. In order to get reliable information regarding mass changes these regions need to be filled. The simplest way is to assume stable conditions in the accumulation regions and substitute missing pixel values by 0 (Pieczonka et al., 2013). Shangguan et al. (2014) classified the elevation differences in terms of elevation bands and replaced missing pixel values by the mean of the elevation differences in the respective elevation band. However, this method only works properly when the sample size of existing pixels is sufficiently large. Surazakov and Aizen (2006) proposed a linear interpolation using TINs assuming stable conditions only at the upper boundaries of the accumulation regions; though, this does not take the non-linear relationship between glacier thickness changes at the glacier front and at the glacier head (Schwitter and Raymond, 1993) into account. Here we considered the non-linear behavior by applying an elevation dependent outlier filtering in order to eliminate erroneous elevation differences on glaciated terrain and filled occurring data gaps by means of ordinary kriging.

5.1. Area changes

The observed shrinkage rates are comparatively small and for most regions within the calculated uncertainty. However, clearly visible retreats at most glacier termini are prevailing. Our results, showing an area decrease at a rate of ~0.05–0.27% a^{-1}, are in agreement with several previous published results proving low rates of glacier shrinkage in the Central Tien Shan, e.g. 0.35% a^{-1} between the mid-1960s and 2000 for the western Chinese Tien Shan (Shangguan et al., 2009) and 0.2% a^{-1} in the 1990–2010 period for the Sary-Djaz Catchment (Osmonov et al., 2013). Slightly higher rates (up to ~0.40% a^{-1}) were observed at adjacent ranges, e.g. Terskey Ala-Too, for the last decades (Narama et al., 2010 [0.4% a^{-1} in the 1970–2000 period], Kutuzov and Shahgedanova, 2009 [0.3% a^{-1} in the 1965–2003 period]). Aizen et al. (2007) reported rates of −0.33% a^{-1} for the entire Ak-Shirak for the 1977–2003 period based on topographic maps and ASTER data which is comparable to the rate measured by Kriegel et al. (2013) of −0.34% a^{-1} for the western part of Ak-Shirak for the ~1970 to ~2005 period based on former inventory data and Landsat TM images. Both numbers are similar to our data of $-0.27 \pm 0.15\%\ a^{-1}$. However, the absolute area reported by Aizen et al. (2007) is higher than our values (~406 km^2 [1977] vs. 382 km^2 [1975]). Comparing the reported value of 406 km^2 for 1977 by Aizen et al. (2007) with our value of 348 km^2 for 2008 reveals a shrinkage of ~14%. This is still significantly lower than 23% of glacier wastage reported by Khromova et al. (2003) for the 1977–2001 period but higher than the 8.8% of glacier shrinkage found in the present study.

This study confirms that glacier shrinkage in the Central Tien Shan was the lowest compared to the outer ranges of the mountain range (Sorg et al., 2012; Narama et al., 2010; Niederer et al., 2008; Bolch, 2007).

Compared to other mountain ranges in High Asia the observed shrinkage is also one of the lowest in entire High Mountain Asia (Bolch et al., 2012; Yao et al., 2012). For the eastern Pamir Khromova et al. (2006) determined a glacier area decrease of about 8% between 1978 and 1990 and ~11% for the 1990–2001 period which is significantly higher than 3.7% observed for the Central Tien Shan in the 1975–2008 period. In contrast, no significant area changes are reported for the Karakoram (Bhambri et al., 2013; Minora et al., 2013). This region, however, showed only low or no mass loss during the last decades and long-term irregular behavior (Gardelle et al., 2013; Bolch et al., 2012; Hewitt, 2011).

5.2. Mass changes

The calculated average mass loss for the Central Tien Shan of 8.8 ± 8.5 m w.e. (0.35 ± 0.34 m w.e. a^{-1}) for the 1975–1999 period is within

Table 4
Statistics for stable and glaciated terrain.

Period	$Mean_{Glacier}$ (m)	$STD_{Glacier}$ (m)	$Mean_{stable}$ (m)	$Median_{Stable}$ (m)	STD_{stable} (m)	$NMAD_{stable}$ (m)
~1975–1999	−10.4	18.5	0.0	0.1	9.5	9.8

NMAD … Normalized Median Absolute Deviation.

Table 5
Mass budgets and surface lowering for the debris-covered parts for the ~1975–1999 period and area changes for the 1975–2008 period of selected glaciers. The ELA (equilibrium line altitude) was derived from snow line values specified in the Katalog Lednikov SSSR [Glacier Inventory of the USSR] (1973) assuming absence of superimposed ice. With regard to the observed rise of temperature an ELA shift of ~50 m between 1974 and 1999 was considered.

ID	Glacier	GLIMS_ID	Area (km^2)	Min elev. (m)	ELA (m)	$MB_{AccumKrig}$ (m w.e. a^{-1})	Δh_{Debris} (m a^{-1})	$\Delta a\ a^{-1}$ [%]
1	Karabatkak	G078275E42138N	2.5	3334	3880	−0.54 ± 0.25	n.a.	−0.11 ± 0.10
2	Bordu-Juschnaja	G078163E41793N	6.9	3750	4240	−0.79 ± 0.25	n.a.	−0.18 ± 0.09
3	Sary-Tor	G078181E41826N	3.4	3837	4240	−0.51 ± 0.25	n.a.	−0.49 ± 0.16
4	Petrov	G078298E41878N	63.5	3729	4240	−0.59 ± 0.25	n.a.	−0.10 ± 0.09
5	Kaindy (Ak-Shirak)	G078303E41787N	20.6	3796	4350	−0.64 ± 0.35	n.a.	−0.24 ± 0.09
6	Dschamansu	G078362E41897N	24.2	3624	4260	−0.68 ± 0.38	n.a.	−0.34 ± 0.08
7	Sauntor	G079101E41716N	9.7	3865	4310	−0.44 ± 0.37	n.a.	−0.13 ± 0.14
8	Bulantor	G079566E42010N	11.9	3571	4310	+0.22 ± 0.42	n.a.	−0.17 ± 0.15
9	Kaindy	G079768E42050N	101.9	3221	4310	−0.27 ± 0.42	−1.25 ± 0.49	−0.14 ± 0.14
10	Samoilowitsch	G079775E41969N	6.7	3263	4310	−0.09 ± 0.42	n.a.	+0.34 ± 0.19[a]
11	Tomur	G079992E41824N	234.9	2631	4450	−0.57 ± 0.48	−1.50 ± 0.56	−0.02 ± 0.08
12	South Inylchek	G080121E42063N	481.5	2897	4420	−0.27 ± 0.45	−0.87 ± 0.53	−0.07 ± 0.05
13	North Inylchek	G080156E42248N	133.7	3327	4420	−0.19 ± 0.45	+0.36 ± 0.53	+0.13 ± 0.08
14	Koxkar	G080106E41800N	63.0	3006	4410	−0.34 ± 0.26	−0.78 ± 0.30	−0.03 ± 0.08
15	Kiqikterang	G080387E41995N	48.4	3067	4340	−0.48 ± 0.30	−0.81 ± 0.35	−0.05 ± 0.10
16	Keqikekuzibayi	G080548E41955N	15.9	3336	4300	+0.02 ± 0.22	−0.49 ± 0.26	−0.04 ± 0.11

The minimum elevation is referring to the 1970s glacier extent.
[a] Glacier surge after 2000.

the global average of 9.7 m w.e. (0.33 m w.e a^{-1}) for the 1976–2005 period derived from glaciological records only (Zemp et al., 2009).

Gardner et al. (2013) reported that the latter, compared to ICESat observations, are prone to be negatively biased. In the present case, however, remote sensing based mass balance assessments and regional estimates from the interpolation of pointwise glaciological records fit well.

The average mass budget is also in agreement with Dyurgerov (2010) who determined a mass loss of 0.38 m w.e. a^{-1} for the 1974–1999 period for the entire Tien Shan mountain range, including outer and inner ranges. He found the highest negative mass budgets during the 1970s (−0.61 m w.e. a^{-1} from 1974 and 1980) and the mid 1990s (−0.65 m w.e. a^{-1} from 1994–1997) falling into our period of investigation.

Our results show that glacier mass loss is lower in the central ranges than in the outer parts of the study region which is also confirmed by observations revealed by Pieczonka et al. (2013) for the region south of Jengish Chokusu and Aizen et al. (2007) for the Ak-Shirak massif. For the latter we found the most pronounced mass loss of 0.51 ± 0.36 m w.e. a^{-1} between 1975 and 1999. In contrast, only moderate mass loss was measured for Inylchek and Tomur region where glacier area changed only insignificantly.

The Ak-Shirak mountain massif has been comprehensively investigated by several studies with special focus on glacier area changes (Engel et al., 2012; Aizen et al., 2007). Mass changes have been specified by Aizen et al. (2007) and Surazakov and Aizen (2006) by means of topographic maps and SRTM3 data. They found a mean thinning for the 1977–1999 period of about 15.1 ± 8.2 m corresponding to a mass loss of 0.59 ± 0.31 m w.e. a^{-1} (when assuming an ice density of 850 kg/m^3) which is in agreement with our result of 0.51 ± 0.36 m w.e. a^{-1}.

For the Tomur area (Chinese side) Pieczonka et al. (2013) determined the overall mass loss for the 1975–1999 period at 0.42 ± 0.23 m w.e. a^{-1} which is slightly higher than the 0.33 ± 0.30 m w.e. a^{-1} determined in this study but still within the uncertainty range. This overestimation is possibly due to the smaller overlap of the utilized KH-9 DTM, where some glaciers west of Koxkar Glacier (e.g. Tomur Glacier) were not entirely covered.

One of the most extensively investigated glaciers in the Chinese part of the Central Tien Shan is Koxkar Glacier, a heavily debris-covered glacier on the southern margin of the mountain range. The mean thinning of Koxkar Glacier has been determined at 0.34 ± 0.26 m a^{-1} for the 1975–1999 period which is in line with the result published by Pieczonka et al. (2013) of 0.41 ± 0.27 m a^{-1}. We also measured the most rapid downwasting for the debris-covered tongue with 0.78 ± 0.30 m a^{-1} which is within the thinning range of 0.5–1.5 m a^{-1} based on repetitive GPR measurements on the glacier tongue conducted in 1981 and 2004 (Xie et al., 2007).

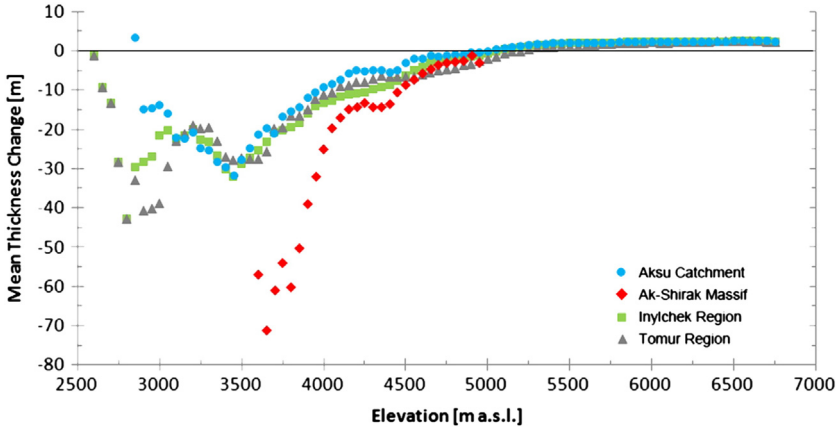

Fig. 6. Mean thickness change calculated in 50 m elevations bands for non-surging glaciers in the Aksu, Tomur, Inylchek, and Ak-Shirak region. Surge-type glaciers have been excluded.

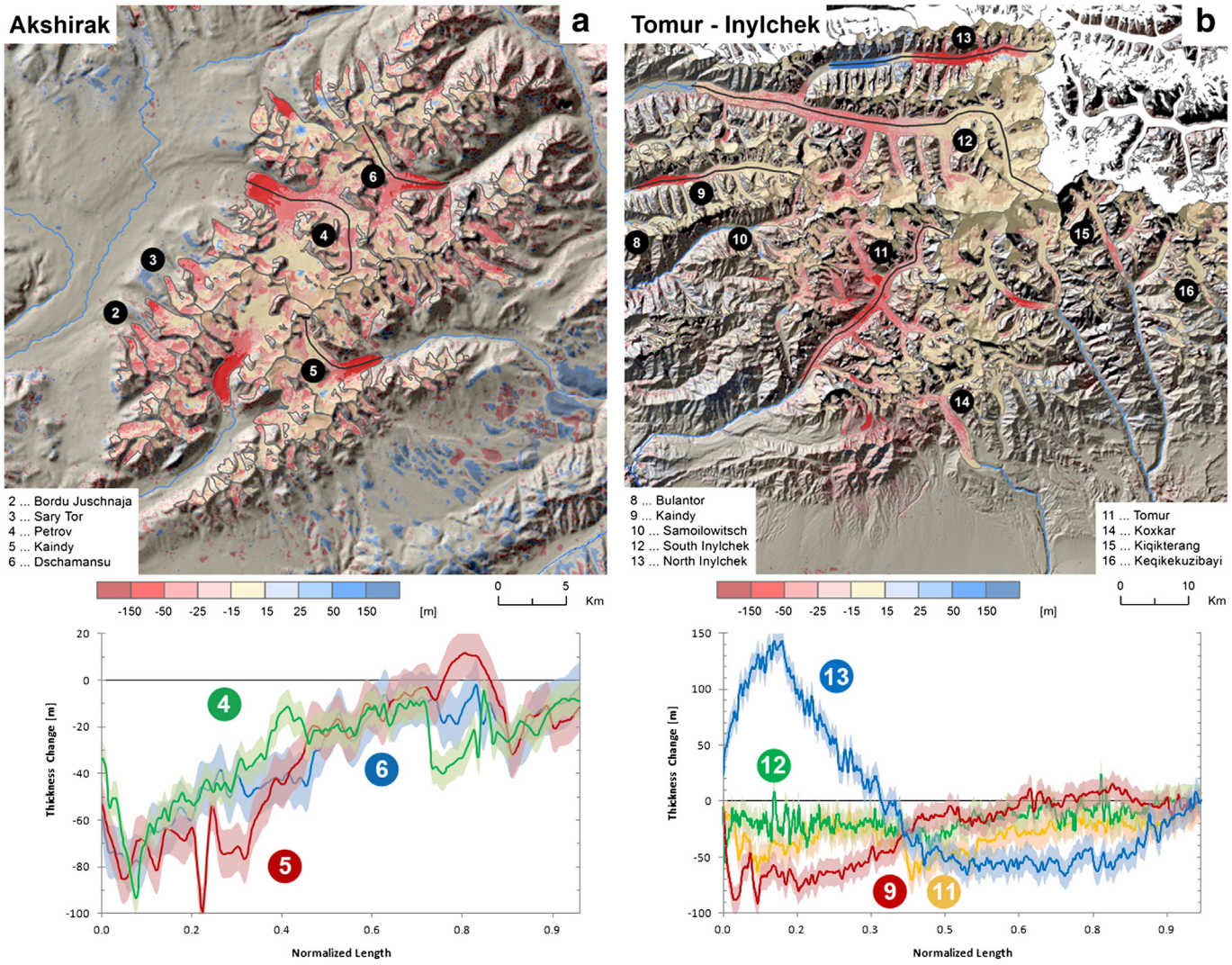

Fig. 7. Difference image between KH-9 Hexagon and SRTM3 for the Ak-Shirak range (left) and Tomur–Inylchek region (right) and longitudinal profiles with normalized length for selected glaciers. The profiles are generated applying a moving average with a bandwidth of 125 m.

Other studies in the region were focusing on single glaciers only. For Qingbingtan Glacier No. 72, for instance, Wang et al. (2011) found an average thickness loss of about 0.22 ± 0.14 m a^{-1} between 1964 and 2008 restricted to the glacier tongue. For the entire glacier we found a less average thinning rate of 0.13 ± 0.47 m a^{-1} for the 1974–1999 period as we are also considering the accumulation region.

In-situ records in the Central Tien Shan are sparse and often limited to short periods. For Sary-Tor Glacier in the western Ak-Shirak massif, for instance, observations are only available for a short period of 5 years in the 1980s (Table 7). Long-term in-situ mass balance measurements are available for Karabatkak Glacier, located on the northern slope of the Terskey Ala-Too (Fig. 2), for the period 1973–1998 (WGMS, 2013). The observed mass budget of −0.61 m w.e. a^{-1} for the 1973–1998 period is consistent with the results of our study of −0.54 ± 0.25 m w.e. a^{-1}.

For the recent decade region wide mass balance estimates are available from gravimetric (GRACE) and laser altimetry (ICESat) measurements (Gardner et al., 2013; Jacob et al., 2012). Extrapolating the average mass loss over the total glacierized area of ~16,500 km^2 (Kotlyakov et al., 2010; Shi et al., 2010) gives a mass balance rate of −6.1 ± 5.8 Gt a^{-1} for the 1975–1999 period which is slightly higher than the −5 ± 6 Gt a^{-1} for the 2003–2010 period found by Jacob et al. (2012) using GRACE data, but the uncertainties are high.

Gardner et al. (2013) found an average surface lowering rate of 0.58 ± 0.21 m a^{-1} (0.49 ± 0.18 m w.e. a^{-1}) between 2003 and 2009 by analyzing ICESat footprints for the entire Tien Shan. This is,

Table 6
Specific mass budgets for selected mountain ranges for the ~1975–1999 period based on KH-9 Hexagon and SRTM3.

Mountain range	Glacier no. (area)	<1 (km^2)	≥1–<5 (km^2)	≥5 (km^2)	$MB_{AccumKrig}$
Ak-Shirak	171 (383 km^2)	66% (38 km^2)	23% (90 km^2)	11% (255 km^2)	−0.51 ± 0.36
Aksu/Sary-Djaz Catch.	1600 (2556 km^2)	76% (336 km^2)	19% (528 km^2)	5% (1692 km^2)	−0.35 ± 0.34
Inylchek area	485 (1117 km^2)	83% (125 km^2)	15% (147 km^2)	2% (845 km^2)	−0.20 ± 0.44
Tomur area	251 (953 km^2)	66% (46 km^2)	26% (140 km^2)	8% (767 km^2)	−0.33 ± 0.30

Assumed ice density 850 kg/m^3; MB in m w.e. a^{-1}.

Table 7
Comparison of in-situ and remote sensing based specific mass budgets.

Glacier	Reference period	Mass budget	Period	Mass budget
Karabatkak	1973–1998	−0.61 m w.e. a^{-1} [b]	1973–1999	−0.54 ± 0.25 m w.e. a^{-1} [a]
Sary-Tor	1984–1989	−0.13 m w.e. a^{-1} [b]	1973–1999	−0.51 ± 0.25 m w.e. a^{-1} [a]

[a] Ice density 850 kg/m^3.
[b] WGMS 2013.

though within the uncertainty range, larger than our downwasting rate of 0.41 ± 0.40 m a^{-1} (0.35 ± 0.34 m w.e. a^{-1}) for the Central Tien Shan for the 1975–1999 period. However, for the recent decade Pieczonka et al. (2013) and Shangguan et al. (2014) found decelerated mass loss for the Tomur and Inylchek region of about 0.2 m w.e. a^{-1} (1999–2009).

The overall spatial pattern of the observed mass changes is comparable to that of the measured glacier area changes, with the most significant loss of glacier area of 8.8 ± 4.8% in the Ak-Shirak massif in the Inner Tien Shan, despite delayed response times. However, on individual glacier basis the area change cannot be well related to mass changes (Table 5). This is especially the case for strongly debris-covered and surge-type glaciers, e.g. the highly debris-covered Southern Inylchek, Tomur and Koxkar Glacier had significant mass loss but only little glacier shrinkage. In contrast, Northern Inylchek Glacier had a significant area increase due to a surge event but an overall mass loss. It is important to underline the fact that mass changes in the Central Tien Shan region are within the global average but area changes are significantly below the mean for the Tien Shan. This highlights that volume and mass change estimates based on the glacier area alone can be considerably biased.

5.3. Climatic considerations and runoff

The melt-regime of the glaciers in the study region is strongly influenced by solar radiation (Aizen et al., 1997b), but several studies have shown that temperature change is the main component controlling glacier evolution in the Tien Shan (Krysanova et al., 2014; Kriegel et al., 2013). This is even more important as Central Tien Shan glaciers receive most of their accumulation during summer due precipitation is concentrated in the warm season (May–September) comparable to Himalayan glaciers. The mean annual air temperature (MAAT) at the Tien Shan Station (3614 m a.s.l.) increased by about 0.01–0.02 °C a^{-1} during the period 1940 and 1991 (Aizen et al., 1997a), with a similar trend thereafter (Kriegel et al., 2013; Osmonov et al., 2013; Bolch, 2006), and 0.02–0.03 °C a^{-1} at Karabatkak Station (3415 m a.s.l.) located close to Issyk-Kul basin (Giese et al., 2007; Kutuzov and Shahgedanova, 2009). In the Chinese part of the Central Tien Shan an increase of about 0.02 °C a^{-1} has been observed since the 1960s (Shangguan et al., 2009; Shi et al., 2007) which is similar to the temperature trend in the Kyrgyz part going along with pronounced changes in glacier mass balance (Cao, 1998). In general, the increase in mean summer air temperature is not more pronounced than the increase in MAAT. However, the magnitude of the temperature change is strongly influenced by the chosen start and end points as shown by Unger-Shayesteh et al. (2013) and Giese et al. (2007).

Trends in annual precipitation were insignificant for the Central Tien Shan during the 1940–1991 period (Aizen et al., 1997a). At the same time, Kriegel et al. (2013) and Osmonov et al. (2013) found decreasing annual precipitation (until 1997) in the Kyrgyz part of the Central Tien Shan towards higher altitudes over the last decades predominantly caused by decreasing summer precipitation.

In contrast, since 1997, when the Tien Shan Station was dislocated, increasing precipitation could be observed. The reliability and comparability of these measurements are, however, questionable as measurement methods have also been changed (Giese et al., 2007). Common to all the studies is the observation that at high altitudes in the Kyrgyz part there is no precipitation increase during the warm season. Increasing precipitation of about ~1 mm a^{-1} since 1961 particularly during the cold season, going along with more accumulation, has been proven for the Chinese part of the Central Tien Shan with uncertainties in high altitude regions due to sparse coverage of weather stations (Krysanova et al., 2014; Wang et al., 2013; Shangguan et al., 2009; Shi et al., 2007).

As a consequence of the observed temperature increase in the study period there is likely less accumulation during the warm period, a plus of energy available for melting processes and a prolongation of the melting season (Narama et al., 2010). These climatic patterns favor accelerated glacier wastage, in particular since the 1970s, as glacier melt exceeds snow accumulation (Cao, 1998). In conclusion, dependent on their size and response time, glaciers will react with more negative mass budgets or accelerating retreat accompanied by an uplift of the equilibrium line altitude (ELA). Aizen (2011), for instance, reported an ELA-uplift of 23 m for the Tien Shan in the 1973–2003 period.

The spatially inhomogeneous climate change is consistent with the observed mass loss with moderate rates in the Chinese part and stronger mass loss in the western part of the study region. Accelerating mass loss in the regions south of Jengish Chokusu as consequence of climate warming is partly counterbalanced by an increase of accumulation in the respective regions.

Annual discharge of Aksu River—in which summer runoff accounts for three quarters of the yearly runoff, whilst winter runoff only accounts for 5% (Fan et al., 2013)—is strongly influenced by the glacial headwaters. Therefore, rising precipitation in the Chinese part and accelerated mass loss in the Kyrgyz part were associated with a pronounced increase in annual runoff in the last decades (Krysanova et al., 2014; Shi et al., 2007; Ye et al., 2006). To calculate the runoff contribution of the glaciers in the Aksu/Sary-Djaz Catchment we extrapolated the measured mass budget over the entire catchment (~2600 km^2) assuming that the average mass loss is also valid for the 675 km^2 which are not covered by the KH-9 DTMs. These results were compared to the discharge at Xiehela Station (Figs. 2 and 5) because the runoff measurements at Xidaquiao Station, located further downstream, might be biased by irrigation activities (Krysanova et al., 2014). The mean annual runoff at Xiehela Station between 1957 and 2003 was measured with 4.87 km^3 a^{-1} (Ye et al., 2006). Under consideration of the average mass loss in the Aksu/Sary-Djaz Catchment of 8.8 m w.e. the annual glacial runoff has been calculated with 0.92 km^3 a^{-1}. Thus, the contribution to the total runoff due to glaciers imbalance at Xiehela Station is roughly ~20% for the 1975–2000 period and more than twice as high as the estimated water contribution due to glaciers imbalance in the second half of the 20th century in the Naryn Catchment, directly north-west of the Aksu Catchment, of ~8% (Hagg et al., 2013). Hence, a significant reduction in runoff can be expected in the long-term as the glacier runoff will reach the turning point with further glacier wastage.

6. Conclusion

The present study revealed continuous glacier mass loss and glacier shrinkage in the Central Tien Shan since the 1970s despite partial thick debris-cover. Since glaciers in the Central Tien Shan receive most of their accumulation during the warm season between May and September glacier mass loss is mainly triggered by an increase of the mean summer and annual air temperatures since the 1970s.

Using declassified KH-9 Hexagon stereo imagery and SRTM3 data a mass loss of 0.35 ± 0.34 m w.e. a^{-1} has been measured in the Central Tien Shan region for the ~1975–1999 period which is not higher than the global average for that period. The highest mass loss could be observed for the Ak-Shirak mountain massif which is about 30% higher than the average for the Central Tien Shan. In contrast, the mass budgets for Inylchek and Tomur region—accommodating large debris-covered glaciers—were roughly half as negative. Downwasting rates of more than 1 m a^{-1} were measured at the debris-covered tongues in the Jengish Chokusu area significantly influencing the overall glacier mass budgets. The glaciers behavior is, however, heterogeneous as some glacier also showed volume gains or surge-type characteristics. The contribution to the overall discharge due to glaciers imbalance is high and has been estimated with ~20% and is likely to increase with further glacier wastage.

The observed spatial pattern of high mass losses in the western and northern parts of the study region and moderate mass losses around the Jengish Chokusu (Tomur Feng)–Khan Tengri massif correlates with comparatively low and partly insignificant glacier shrinkage rates in the region at $-0.27 \pm 0.15\%$ a^{-1} in the Ak-Shirak region and $-0.08 \pm 0.15\%$ a^{-1} in the Tomur region. Glacier shrinkage in the Central Tien Shan was the lowest compared to the outer ranges of the mountain range.

Relatively low glacier shrinkage accompanied by a mass loss being similar to the global average underlines that hydrological conclusions and mass change estimates based on area changes only can be significantly biased.

Author contribution

T.B. and T.P. designed the study. T.P. processed the KH-9 Hexagon imagery and determined the mass budgets. T.B. investigated the glacier area changes and contributed to the writing.

Acknowledgments

This study was conducted in the framework of the project Sustainable Management of River Oases along the Tarim River/China (SuMaRiO) funded by BMBF (Code 01 LL 0918 B) and the bundle project Water Resources in the Aksu-Tarim-River Catchment of Western China and the Effects of Climate Change (AKSU-TARIM) supported by the Deutsche Forschungsgemeinschaft (DFG, Code BO 3199/2-1). We would like to thank Anne-Kathrin Becker, Ulrike Schinke, Cees Jan Cojin, and Azamat Osmonov for their contributions to the glacier inventory data. We acknowledge the cooperation with Liu Shiyin and his group of CAREERI, Lanzhou. We are also grateful to Manfred Buchroithner, Juliane Peters, and Nicolai Holzer from TU Dresden for fruitful discussions.

References

Aizen, V.B., 2011. Tien Shan Glaciers. In: Sigh, V.P., Singh, P. (Eds.), Encyclopedia of Snow, Ice and Glaciers. Haritashya Springer Publisher, U.K., p. 1253.

Aizen, V.B., Aizen, E.M., Melack, J.M., Dozier, J., 1997a. Climatic and hydrologic changes in the Tien Shan, Central Asia. J. Clim. 10 (6), 1393–1404.

Aizen, V.B., Aizen, E.M., Dozier, J., Melack, J.M., Sexton, D.D., Nesterov, V.N., 1997b. Glacial regime of the highest Tien Shan mountain, Pobeda-Khan Tengry massif. J. Glaciol. 43 (145), 503–512.

Aizen, V.B., Kuzmichenok, V.A., Surazakov, A.B., Aizen, E.M., 2007. Glacier changes in the Tien Shan as determined from topographic and remotely sensed data. Glob. Planet. Chang. 56, 328–340.

Arendt, A., Bolch, T., Cogley, J.G., Gardner, A., Hagen, J.-O., Hock, R., Kaser, G., Pfeffer, W.T., Moholdt, G., Paul, F., Radić, V., Andreassen, L., Bajracharya, S., Barrand, N., Beedle, M., Berthier, E., Bhambri, R., Bliss, A., Brown, I., Burgess, D., Burgess, E., Cawkwell, F., Chinn, T., Copland, L., Davies, B., De Abgelis, H., Dolgova, E., Filbert, K., Forester, R.R., Fountain, A., Frey, H., Giffen, B., Glasser, N., Gurney, S., Hagg, W., Hall, D., Haritashya, U.K., Hartmann, G., Helm, C., Herreid, S., Howat, I., Kapustin, G., Khromova, T., Kienholz, C., Köonig, M., Kohler, J., Kriegel, D., Kutuzov, S., Lavrentiev, I., Le Bris, R., Lund, J., Manley, W., Mayer, C., Miles, E., Li, X., Menounos, B., Mercer, A., Mölg, N., Mool, P., Nosenko, G., Negrete, A., Nuth, C., Pettersson, R., Racoviteanu, A., Ranzi, R., Rastner, P., Rau, F., Raup, B., Rich, J., Rott, H., Schneider, C., Seliverstov, Y., Sharp, M., Sigurðsson, O., Stokes, C., Wheate, R., Winsvold, S., Wolken, G., Wyatt, F., Zheltyhina, N., 2012. Randolph Glacier Inventory—A Dataset of Global Glacier Outlines: Version 3.2. Global Land Ice Measurements from Space, Boulder Colorado. Digital Media, USA.

Berthier, E., Schiefer, E., Clarke, G.K.C., Menounos, B., Rémy, F., 2010. Contribution of Alaskan glaciers to sea-level rise derived from satellite imagery. Nat. Geosci. 3, 92–95. http://dx.doi.org/10.1038/NGEO737.

Bhambri, R., Bolch, T., Kawishwar, P., Dobhal, D., Srivastava, D., Pratap, B., 2013. Heterogeneity in glacier response in the Shyok valley, northeast Karakoram. Cryosphere 1384–1398.

Bolch, T., 2006. GIS- und fernerkundungsgestütze Analyse und Visualisierung von Klimaänderung und Gletscherschwund im nördlichen Tien Shan mit einem Vergleich zur Bernina-Gruppe/Alpen. (Ph.D. Thesis). Institut für Geographie, Erlangen, Germany.

Bolch, T., 2007. Climate change and glacier retreat in northern Tien Shan (Kazakhstan/Kyrgyzstan) using remote sensing data. Glob. Planet. Chang. 56, 1–12.

Bolch, T., 2014. Glacier area and mass changes since 1964 in the Ala Archa Valley, Kyrgyz Ala-Too, northern Tien Shan. Ice and Snow (accepted for publication).

Bolch, T., Menounos, B., Wheate, R.D., 2010. Landsat-based inventory of glaciers in western Canada, 1985–2005. Remote Sens. Environ. 114, 127–137.

Bolch, T., Pieczonka, T., Benn, D.I., 2011. Multi-decadal mass loss of glaciers in the Everest area (Nepal Himalaya) derived from stereo imagery. Cryosphere 5, 349–358.

Bolch, T., Kulkarni, A., Kääb, A., Huggel, C., Paul, F., Cogley, J., Frey, H., Kargel, J., Fujita, K., Scheel, M., Bajracharya, S., Stoffel, M., 2012. The state and fate of Himalayan Glaciers. Science 336, 310–314. http://dx.doi.org/10.1126/science.1215828.

Burnett, M.G., 2012. Hexagon (KH-9) Mapping Program and Evolution. National Reconnaissance Office, Chantilly, Virginia.

Cao, M.S., 1998. Detection of abrupt changes in glacier mass balance in the Tien Shan Mountains. J. Glaciol. 44 (147), 352–358.

Dyurgerov, M.B., 2010. Reanalysis of glacier changes: from the IGY to the IPY, 1960–2008. Data Glaciol. Stud. 108, 1–116.

Engel, Z., Šobr, M., Yerokhin, S., 2012. Changes of Petrov glacier and its proglacial lake in the Akshiirak massif, central Tien Shan, since 1977. J. Glaciol. 58 (208), 388–398.

Fan, Y., Chen, Y., Liu, Y., Li, W., 2013. Variation of baseflows in the headstreams of the Tarim River Basin during 1960–2007. J. Hydrol. 487, 98–108.

Gardelle, J., Berthier, E., Arnaud, Y., Kääb, A., 2013. Region-Wide Glacier Mass Balances Over the Pamir–Karakoram–Himalaya During 1999–2011. , pp. 1999–2011.

Gardner, A.S., Moholdt, G., Cogley, J.G., Wouters, B., Arendt, A.A., Wahr, J., Berthier, E., Hock, R., Pfeffer, W.T., Kaser, G., Ligtenberg, S.R.M., Bolch, T., Sharp, M.J., Hagen, J.O., van den Broeke, M.R., Paul, F., 2013. A reconciled estimate of glacier contributions to sea level rise: 2003 to 2009. Science 340, 852–857. http://dx.doi.org/10.1126/science.1234532.

Giese, E., Mossig, I., Rybski, D., Bunde, A., 2007. Long-term analysis of air temperature trend in Central Asia. Erdkunde 61, 186–202.

Hagg, W., Mayer, C., Lambrecht, A., Kriegel, D., Azizov, E., 2013. Glacier changes in the Big Naryn basin, Central Tien Shan. Glob. Planet. Chang. 110, 40–50.

Hewitt, K., 2011. Glacier change, concentration, and elevation effects in the Karakoram Himalaya, Upper Indus Basin. Mt. Res. Dev. 33, 188–200.

Huss, M., 2013. Density assumptions for converting geodetic glacier volume change to mass change. The Cryosphere, 7, 877-887. Cryosphere 7, 1263–1286.

Jacob, T., Wahr, J., Pfeffer, W., Swenson, S., 2012. Recent contributions of glaciers and ice caps to sea level rise. Nature 482, 514–518. http://dx.doi.org/10.1038/nature10847.

Jacobsen, K., 2005. DEMs based on space images versus SRTM height models. Proc. ASPRS 2005 Annual Conference, Baltimore, Maryland, March 07-11, 2005.

Jarvis, A., Reuter, H.I., Nelson, A., Guevara, E., 2008. Hole-filled SRTM for globe Version 4. (available from the CGIAR_CSI SRTM 90 m, database). http://srtm.csi.cgiar.org.

Juen, M., Mayer, C., Lambrecht, A., Han, H., Liu, S., 2014. Impact of varying debris cover thickness on ablation: a case study for Koxkar Glacier in the Tien Shan. Cryosphere 8, 377–386.

Kääb, A., Berthier, E., Nuth, C., Gardelle, J., Arnaud, Y., 2012. Contrasting patterns of early twenty-first-century glacier mass change in the Himalayas. Nature 488, 495–498.

Kaser, G., Grosshauser, M., Marzeion, B., 2010. Contribution potential of glaciers to water availability in different climate regimes. Proc. Natl. Acad. Sci. 107, 20223–20227.

Katalog Lednikov SSSR [Glacier Inventory of the USSR], 1973. Centralnaya Aziaya [Central Asia], Tom 14 V 2 KyrgyzstanPart 2. Hydrometeoizdat, Leningrad (in Russian).

Khromova, T.E., Dyurgerov, M.B., Barry, R.G., 2003. Late twentieth century changes in glacier extent in the Akshirak Range, Central Asia, determined from historical data and ASTER imagery. Geophys. Res. Lett. 30, 1863.

Khromova, T.E., Osipova, G.B., Tsvetkov, D.G., Dyurgerov, M.B., Barry, R.G., 2006. Changes in glacier extent in the eastern Pamir, Central Asia, determined from historical data and ASTER imagery. Remote Sens. Environ. 102, 24–32.

Khromova, T., Nosenko, G., Kutuzov, S., Maraviev, A., Chernova, L., 2014. Glacier area changes in Northern Eurasia. Environ. Res. Lett. 9. http://dx.doi.org/10.1088/1748-9326/9/1/015003.

Kotlyakov, V.M., Dyakova, A.M., Koryakin, V.S., Kravtsova, V.I., Osipova, G.B., Varnakova, G.M., Vinogradov, V.N., Vinogradov, O.N., Zverkova, N.M., 2010. Glaciers of Asia—Glaciers of the Former Soviet Union. In: Williams, R.S., Ferrigno, J.G. (Eds.), Sattelite Image Atlas of Glaciers of the World. U.S. Geological Survey Professional Paper, p. 1386-F-1.

Kriegel, D., Mayer, C., Hagg, W., Vorogushyn, S., Duethmann, D., Gafurov, A., Farinotti, D., 2013. Changes in glacierisation, climate and runoff in the second half of the 20th century in the Naryn basin, Central Asia. Glob. Planet. Chang. 110, 51–61. http://dx.doi.org/10.1016/j.gloplacha.2013.05.014.

Krysanova, V., Wortmann, M., Bolch, T., Merz, B., Duethmann, D., Walter, J., Huang, S., Tong, J., Buda, Su., Kundzewicz, Z.W., 2014. Analysis of current trends in climate parameters, river discharge and glaciers in the Aksu River basin (Central Asia). Hydrol. Sci. J. http://dx.doi.org/10.1080/02626667.2014.925559.

Kutuzov, S., 2012. Glacier area and volume changes in the Terskei Ala-Tau Range for the second part of XX century. Ice and Snow V. 1, pp. 5–15 (in Russian).
Kutuzov, S., Shahgedanova, M., 2009. Glacier retreat and climatic variability in the eastern Terskey-Alatoo, inner Tien Shan between the middle of the 19th century and beginning of the 21st century. Glob. Planet. Chang. 69, 59–70.
Lamsal, D., Sawagaki, T., Watanabe, T., 2011. Digital terrain modelling using corona and ALOS PRISM data to investigate the distal part of Imja Glacier, Khumbu Himal, Nepal. J. Mt. Sci. 8, 390–402. http://dx.doi.org/10.1007/s11629-011-2064-0.
Marzeion, B., Cogley, J.G., Richter, K., Parkes, D., 2014. Attribution of global glacier mass loss to anthropogenic and natural causes. Science 345, 919–921.
Mavlyudov, B.R., 1999. Inylchek Glacier and the Merzbacher Lake: situation in 1997. Data Glaciol. Stud. 86, 142–148 (in Russian).
Minora, U., Bocchiola, D., D'Agata, C., Maragno, D., Mayer, C., Lambrecht, A., Mosconi, B., Vuillermoz, E., Senese, A., Compostella, C., Smiraglia, C., Diolaiuti, G., 2013. 2001–2010 glacier changes in the Central Karakoram National Park: a contribution to evaluate the magnitude and rate of the "Karakoram anomaly". Cryosphere Discuss. 7, 2891–2941.
Mollberg, B.H., Schardt, B.B., 1988. Mission report on the Orbiter Camera Payload System (OCPS) Large Format Camera (LFC) and Attitude Reference System (ARS). NASA, Houston, Texas.
Narama, C., Kääb, A., Duishonakunov, M., Abdrakhmatov, K., 2010. Spatial variability of recent glacier area changes in the Tien Shan Mountaints, Central Asia, using Corona (~1970), Landsat (~2000), and ALOS (~2007) satellite data. Glob. Planet. Chang. 71, 42–54.
Niederer, P., Bilenko, V., Ershova, N., Hurni, H., Yerokhin, S., Maselli, D., 2008. Tracing glacier wastage in the Northern Tien Shan (Kyrgyzstan/Central Asia) over the last 40 years. Clim. Chang. 86, 227–234.
Nuth, C., Kääb, A., 2011. Co-registration and bias corrections of satellite elevation data sets for quantifying glacier thickness change. Cryosphere 5, 271–290.
Oerelemans, J., 2001. Glaciers and Climate Change. A. A. Balkema Publishers, Rotterdam.
Osmonov, A., Bolch, T., Xi, C., Kurban, A., Guo, W., 2013. Glacier characteristics and changes in the Sary-Djaz River Basin (Central Tien Shan, Kyrgyzstan)—1990–2010. Remote Sens. Lett. 4 (8), 725–734.
Paul, F., Haeberli, W., 2008. Spatial variability of glacier elevation changes in the Swiss Alps obtained from two digital elevation models. Geophys. Res. Lett. 35 L21502.
Paul, F., Kääb, A., Maisch, M., Kellenberger, T., Haeberli, W., 2002. The new remote sensing derived Swiss Glacier Inventory: I. Methods Ann. Glaciol. 34, 355–361.
Paul, F., Barrand, N.E., Baumann, S., Berthier, E., Bolch, T., Casey, K., Frey, H., Joshi, S.P., Konovalov, V., Le Bris, R., Mölg, N., Nosenko, G., Nuth, C., Pope, A., Racoviteanu, A., Rastner, P., Raup, B., Scharrer, K., Steffen, S., Winsvold, S., 2013. On the accuracy of glacier outlines derived from remote-sensing data. Ann. Glaciol. 54 (63), 171–182.
Paul, F., Bolch, T., Kääb, A., Nagler, T., Nuth, C., Scharrer, K., Shepherd, A., Strozzi, T., Ticconi, F., Bhambri, R., Berthier, E., Bevan, S., Gourmelen, N., Heid, T., Jeong, S., Kunz, M., Lauknes, T.R., Luckman, A., Merryman Boncori, L.P., Moholdt, G., Muir, A., Neelmeijer, J., Rankl, M., VanLooy, J., Van Niel, T., 2014. The glaciers climate change initiative: methods for creating glacier area, elevation change and velocity products. Remote Sens. Environ. http://dx.doi.org/10.1016/j.rse.2013.07.043.
Pieczonka, T., Bolch, T., Buchroithner, M., 2011. Generation and evaluation of multitemporal digital terrain models of the Mt. Everest area from different optical sensors. ISPRS J. Photogramm. Remote Sens. 66, 927–940.
Pieczonka, T., Bolch, T., Wie, J., Liu, S., 2013. Heterogeneous mass loss of glaciers in the Aksu-Tarim Catchment (Central Tien Shan) revealed by 1976 KH-9 Hexagon and 2009 SPOT-5 stereo imagery. Remote Sens. Environ. 130, 233–244.
Racoviteanu, A.E., Manley, W.F., Arnaud, Y., Williams, M.W., 2007. Evaluating digital elevation models for glaciologic applications: an example from Nevado Coropuna, Peruvian Andes. Glob. Planet. Chang. 59, 110–125.
Rignot, E., Echelmeyer, K., Krabill, W., 2001. Penetration depth of interferometric synthetic-aperture radar signals in snow and ice. Geophys. Res. Lett. 28 (18), 3501–3504.
Rodriguez, E., Morris, C.S., Belz, J.E., 2006. A global assessment of the SRTM performance. Photogramm. Eng. Remote. Sens. 72, 249–260.
Sakai, A., Takeuchi, N., Fujita, K., Nakawo, M., 2000. Role of supraglacial ponds in the ablation process of a debris-covered glacier in the Nepal Himalayas. Debris Covered Glaciers, IAHS Publications. 265, pp. 119–132.
Schiefer, E., Menounos, B., Wheate, R., 2007. Recent volume loss of British Columbian glaciers, Canada. Geophys. Res. Lett. 34. http://dx.doi.org/10.1029/2007GL030780 L16503.
Schwitter, M.P., Raymond, C.F., 1993. Changes in the longitudinal profiles of glaciers during advance and retreat. J. Glaciol. 39 (133), 582–590.
Shangguan, D., Liu, S., Ding, Y., Ding, L., Xu, J., Jing, L., 2009. Glacier changes during the last forty years in the Tarim Interior River basin, northwest China. Prog. Nat. Sci. 19, 727–732.
Shangguan, D., Bolch, T., Ding, Y., Kröhnert, M., Pieczonka, T., Wetzel, H.-U., Liu, S., 2014. Elevation changes of Inylchek Glacier during 1974–2007, Central Tian Shan, Kyrgyzstan derived from remote sensing data. Cryosphere Discuss. 8, 1–38.
Shi, Y., Liu, S., 2000. Estimation on the response of glaciers in China to the global warming in the 21st century. Chin. Sci. Bull. 45, 668–672.
Shi, Y., Shen, Y., Kang, E., Li, D., Ding, Y., Zhang, G., Hu, R., 2007. Recent and future climate change in northwest China. Clim. Chang. 80, 379–393. http://dx.doi.org/10.1007/s10584-006-9121-7.
Shi, Y., Mi, D., Yao, T., Zeng, Q., Liu, C., 2010. Glaciers of Asia—Glaciers of China. In: Williams, R.S., Ferrigno, J.G. (Eds.), Satellite Image Atlas of Glaciers of the World. U.S. Geological Survey Professional Paper, p. 1386-F-2.
Sorg, A., Bolch, T., Stoffel, M., Solomina, O., Beniston, M., 2012. Climate change impacts on glaciers and runoff in Tien Shan (Central Asia). Nat. Clim. Chang. 2, 725–731.
Surazakov, A., Aizen, V.B., 2006. Estimating volume change of mountain glaciers using SRTM and map-based topographic data. IEEE Trans. Geosci. Remote Sens. 44 (10), 2991–2995.
Surazakov, A., Aizen, V.B., 2010. Positional accuracy evaluation of declassified Hexagon KH-9 mapping camera imagery. Photogramm. Eng. Remote. Sens. 76 (5), 603–608.
Unger-Shayesteh, K., Vorogushyn, S., Farinotti, D., Gafurov, A., 2013. What do we know about past changes in the water cycle of Central Asian headwaters? A review. Glob. Planet. Chang. 110, 4–25.
Wang, S., Wang, Y., Wang, J., Mao, W., Shen, Y., 2003. Change of climate and hydrology in the Tarim River basin during past 40 years and their impact. J. Glaciol. Geocryol. 25 (3), 315–320.
Wang, P., Li, Z., Li, H., Wang, W., Wang, F., 2011. Ice surface-elevation change and velocity of Qingbingtan Glacier No. 72 in the Tomor Region, Tianshan Mountains, Central Asia. J. Mt. Sci. 8, 855–864.
Wang, P., Li, Z., Wang, W., Li, H., Zhou, P., Jin, S., 2013. Changes of six selected glaciers in the Tomor region, Tian Shan, Central Asia, over the past 50 years, using high-resolution remote sensing images and field surveying. Quat. Int. 1–9.
WGMS., 2013. Glacier Mass Balance Bulletin No. 12 (2010–2011). In: Zemp, M., Nussbaum, S.U., m Naegeli, K., Gärtner-Roer, I., Paul, F., Hoelzle, M., Haeberli, W. (Eds.), ICSU (WDS)/IUGG (IACS)/UNEP/UNESCO/WMO. World Glacier Monitoring Service, Zurich http://dx.doi.org/10.5904/wgms-fog-2013-11 (106 pp., publication based on database version).
Xie, C., Ding, Y., Chen, C., Han, T., 2007. Study on the change of Keqikaer Glacier during the last 30 years, Mt. Tuomuer, Western China. Environ. Geol. 51, 1165–1170.
Xiuping, J., Richards, J.A., 1999. Remote Sensing Digital Image Analysis: An Introduction. 3rd ed. Springer, New York.
Yao, T., Thompson, L.G., Yang, W., Yu, W., Gao, Y., Guol, X., Yang, X., Duan, K., Zhao, H., Xu, B., Pu, J., Lu, A., Xian, Y., Kattel, D.B., Joswiak, D., 2012. Different glacier status with atmospheric circulations in Tibetan Plateau and surroundings. Nat. Clim. Chang. 2, 663–667.
Ye, M., Xu, H., Song, Y., 2006. The utilization of water resources and its variation tendency in Tarim River Basin. Chin. Sci. Bull. 51, 16–24. http://dx.doi.org/10.1007/s11434-006-8203-2.
Zemp, M., Hoelzle, M., Haeberli, W., 2009. Six decades of glacier mass balance observations—a review of the worldwide monitoring network. Ann. Glaciol. 50, 101–111.